

EFFECT OF ERBIUM DOPING ON PHYSICAL PROPERTIES OF LaFeO₃

J. Ahmad^{1,*}, K. A. Rao¹, J. A. Khan¹, S. H. Bukhari², M. T. Jamil¹, U. Nissar¹, H. Abbas¹, T. Sultan³ and A. Latif³

¹ Department of Physics, Bahauddin Zakariya University, Multan 60800, Pakistan

² Department of Physics, GC University Faisalabad, Sub-Campus, Layyah 31200, Pakistan

³ Department of Civil Engineering, Bahauddin Zakariya University, Multan 6800, Pakistan

* Corresponding Author: javedahmad@bzu.edu.pk, dr.j.ahmad@gmail.com

ABSTRACT: Multiferroic La_{1-x}Er_xFeO₃ (x= 0, 0.2, 0.4, 0.6, 0.8 and 1) successfully synthesized using auto combustion sol-gel citrate method. The crystalline structure examined by X-ray Diffraction (XRD) analysis is orthorhombic. Infrared (IR) active phonons for Erbium substitution in La_{1-x}Er_xFeO₃ studied at room temperature in frequency range 30-1000 cm⁻¹ via Fourier transformed infrared (FTIR) spectroscopy. The experimental reflectivity spectra has been fitted using Lorentz oscillator model and obtain the parameter like damping factor, optical frequency as well as oscillator strength. Real and imaginary part of dielectric constant, optical conductivity, loss function and energy band gap in addition to transverse and longitudinal optical frequency modes have been calculated by these parameters. The frequency shift has been observed with doping concentration of Erbium in LaFeO₃. Optical conductivity spectra are of semiconducting type. La_{1-x}Er_xFeO₃ is further characterized by UV-visible spectroscopy and electrical resistivity measurements. The optical spectrum of UV-Visible phenomena exhibits typical semiconductor behaviour. Investigation shows there is a drop in activation energy of samples if doped element Er increases. The electrical resistivity trend shows semiconducting behaviour of the sample which exhibit p-type polaronic conduction.

Keywords: X-ray diffraction; Fourier Transform Infrared Spectroscopy (FTIR); UV-visible spectroscopy; Electrical resistivity.

(Received 05.01.2021

Accepted 24.03.2021)

INTRODUCTION

Among rare earth orthorhombic materials, mostly LaFeO₃ have studied due to fascinating characteristics as its thermal expansion coefficient is low, stable across a wide temperature range is high, and remarkable low cost of synthesis (Wang & Kang, 2002). LaFeO₃ has excellent photo catalytic activity under visible light and also used in gas sensors (Tijare *et al*, 2012). Regardless of wide range of utilization, many attempts were concerned for the development of lanthanum based ferrite properties. The purpose is to develop higher performing material which is essential for the composition of multifunctional devices. The doping of trivalent or divalent cation into ferrite sub lattices is most adopted preferences (Zhang, Hu, Song, Qin, & Jiang, 2006). The objective is to create the defects in LaFeO₃ crystal structure that affects lattice structure, transport properties, thermal stability and also electronic disorder. Various properties were observed due to doping of elements such as cadmium, antimony (Andoulsi, Horchani-Naifer, & Ferid, 2013) and bismuth. In LaFeO₃, electrochemical and catalytic properties were enhanced by replacement of iron by transition metal ion (Hosseini *et al*, 2010). Magnetic and electrical properties in LaFeO₃ were investigated by replacement of lanthanum from rare earth elements.

LaFeO₃ with substitution of transition metals (e.g. Cr, Co) have been studied (Mahmood, Warsi, Ashiq, & Ishaq, 2013). Because of their thermal stability and sensitivity, they are typically utilize as e-noses for the examination of ailment by usage the gas sensing characteristics (Zhang, Qin, Song, Hu, & Jiang, 2006). LaFeO₃ being a part of ABO₃ perovskite family in which A-side have a cation of large size and Fe atom surrounded by six oxygen atom. These materials show the transition from paramagnetic to antiferromagnetic at 150 K. Synthesis techniques are essential for the formation of uninterrupted LaFeO₃. Naturally, the two phases are considered rhombohedral (*R3c*) and orthorhombic (*Pnma*) present and exhibit paramagnetic behavior (Q. Huang *et al*, 1998). Er is a six-sided square showing anti-ferromagnetic at T_N = 80 K low temperature and T_N = 914 K for ferroelectricity at high temperatures (Katsufuji *et al*, 2001). With ferroelectricity, there is a need for a blank d-shell and magnetism full of d-shell, showing as it does d⁰ vs d_n (Eerenstein, Mathur, & Scott, 2006). Ferromagnetic materials are used to build objects with a high dielectric value and a capacitor. The tangent loss in addition to the dielectric continuity is discussed in the combination of a combination of magneto resistive and electrical magneto in six small-case cases (Z. J. Huang, Cao, Sun, Xue, & Chu, 1997). Due to strong interplay between ferroelectric order, symmetry issues in

phase transformation and magnetic frustration arouse remarkable interest in multiferrocity which tends to characterize these materials (Tamerd *et al*, 2016).

These efforts inspired us to make the doping of Erbium of various concentrations and investigate the lattice dynamics, electrical and optical behaviour. We report in this work the structural, optical and transport properties of $\text{La}_{1-x}\text{Er}_x\text{FeO}_3$ ($x= 0.2, 0.4, 0.6, 0.8, 1$) solid solutions.

MATERIALS AND METHODS

By adopting sol gel method, the composites of ErFeO_3 and LaFeO_3 having polycrystalline was prepared after achieving homogenous solution. It was annealed for two hours at **1000** °C (Hench & West, 1990).The dry blackish powder was grinded by hand in agate mortar. As a binder polyvinyl alcohol (PVA), was used. This sample attained 30 KN pressure to made the pellets by using hydraulic process (Sahoo, Das, & Nath, 2018). For analyzing phase nature of obtained samples X-ray analysis (Bruker D8 advance diffractometer with Cu-K α source) has been used to study chemical and structural composition the S-5200 Ultra-high resolution (Hitachi) was used having magnification of 80 K. For IR measurement at room temperature Fourier transform IR spectrometer (Vertex 80v) has been used in the near normal incidence mode. The range of 30 – 7500 cm^{-1} was covered by assembling KBR-DLaTGS and Mylar and 6 μm -DLaTGS two beam splitter detector combinations (J Ahmad *et al*, 2019; Khan & Ahmad, 2019). The display spectrum used was obtained using a UV reflective Perkin Elmer Lambda 950 UV / VIS / NIR region spectrophotometer (200-850 nm) wavelength region. Electrical resistivity graphs have been measured by using Keithley 2400 source meter with voltage upto 20 V using two point probe method.

RESULTS AND DISCUSSIONS

X-ray Diffraction: X-ray diffraction is a useful method for determining the crystal structure of an atomic element. We therefore investigate the LEFO separation pattern in ($x = 0, 0.2, 0.4, 0.6, 0.8$ and 1) represented in the figure 1 to evaluate the whole structure and properties of the sample. There are many areas related to structure e.g. grain size, lattice parameters and space group can be determined from XRD. High values of $x = 0$ polycrystalline LaFeO_3 (Lanthanum Iron oxide) and $x = 1$ ErFeO_3 (Erbium Iron oxide) matched (with JCPDS card No. 74-2203 and JCPDS card No. 01-072-1281), respectively, that having an orthorhombic perovskite structure consisting of Pbnm space group and space group no. 62 (Hench & West, 1990). The sample exhibits the highly crystalline nature due to narrow and sharp

peaks of powder illustrate by diffraction pattern. To compare these spectrum with standard JCPDS cards, the spectrum at $x= 0.2, 0.4, 0.6, 0.8$ manifest best matching with SG 62.

FTIR Analysis: The room temperature reflectivity spectra of polycrystalline $\text{La}_{1-x}\text{Er}_x\text{FeO}_3$ has been measured at in normal incidence mode having frequency range 30-1000 cm^{-1} . In these spectra, we have observed many kinks in low frequency region and signal to noise ratio is high for high frequency part, therefore, is structure less and is due to absence of electronic excitation. The information about transition from lower quantum state to higher quantum state can be done by calculating oscillating strength. We analyzed IR spectra by using two techniques i.e. Kramer – Kroning (KK) transformation and other is dispersion model (Classical Drude-Lorentz oscillator). Lorentz oscillator model is used to fit and understand the reflectivity spectra (M Zaghrioui, Phuoc, Souza, & Gervais, 2008).

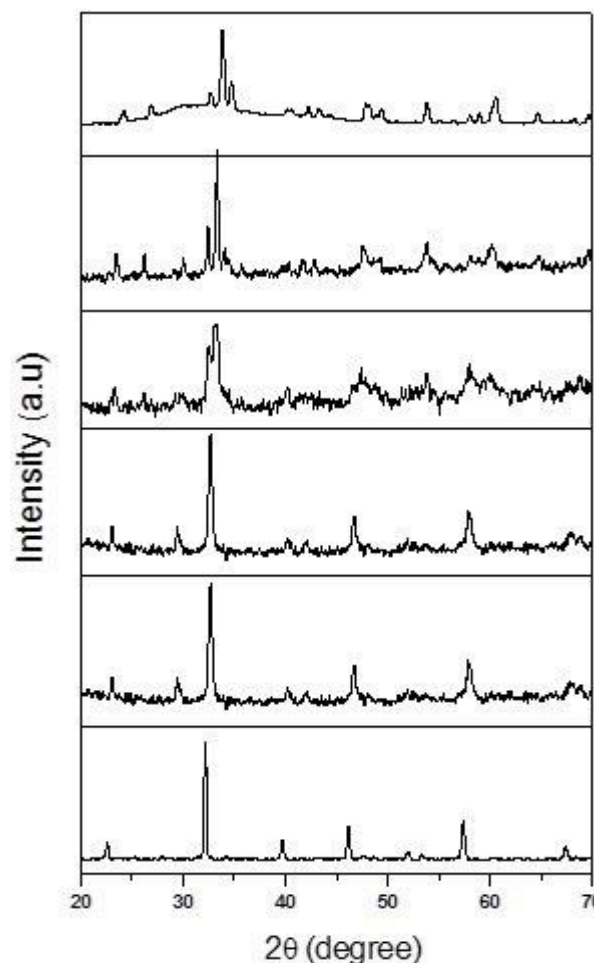


Fig. 1. The X-ray diffraction pattern for $\text{La}_{1-x}\text{Er}_x\text{FeO}_3$ at ($x=0, 0.2, 0.4, 0.6, 0.8$ and 1).

The dielectric function $\epsilon(\omega)$ is define as

$$\epsilon(\omega) = \epsilon_{\infty} + \sum_j \frac{\omega_{TO(j)}^2 S_j}{\omega_{TO(j)}^2 + \omega^2 + i\omega\gamma_j} \quad (1)$$

where $\epsilon(\omega)$ is complex dielectric constant with frequency dependence, j is total number of phonons, $\omega_{TO(j)}$ phonon frequency for j^{th} transverse optical (TO) phonon, γ_j is damping factor and S_j is oscillating strength for j^{th} transverse optical (TO) phonon mode, respectively. The relation related to reflectivity to dielectric constant is

$$R(\omega) = \left| \frac{\sqrt{\epsilon(\omega)} - 1}{\sqrt{\epsilon(\omega)} + 1} \right|^2 \quad (2)$$

The theoretically observed phonons for ABO₃ perovskite structure are 25 IR phonons modes (9B_{1u} + 7B_{2u} + 9B_{3u}) (Bukhari & Ahmad, 2016; Iliev, Abrashev, Popov, & Hadjiev, 2003). By analyzing the calculated spectra of each sample, we have observed 9 phonons for x=0 and 11 intermediate as well as 12 for x=0.8 and maximum number of phonons related to x = 1. The difference in theoretical and experimental regarding phonons is due to polycrystals nature of samples. Phonon modes are categorized into three phonon bands, first one is external mode ($\omega < 290 \text{ cm}^{-1}$), intermediate range known as bending mode ($290 \text{ cm}^{-1} < \omega < 590 \text{ cm}^{-1}$) and

high frequency phonons termed as stretching modes ($\omega > 590 \text{ cm}^{-1}$) (Alter & Nakatsuji, 1996). The primary oxygen ion vibration is referred as bending (intermediate frequency range) and stretching modes (high frequency range) and motion of FeO₆ as well as La is referred as external mode. The reflectivity spectrum of LaFeO₃ has 9 modes that are at 85, 172, 269, 292, 332, 386, 417, 428 and 541 cm⁻¹. The phonon observed at 85 cm⁻¹ involve motion of La atoms relative to FeO₆ octahedra. The heaviest atom of considered compound exhibits vibration in region of low wavenumber (According to harmonic oscillator Approximation) (Jamil, Ahmad, Bukhari, & Ahmad, 2018). In external modes, three phones ranging from 85, 172 and 269 cm⁻¹ that is due to the La atomic movement relative to the octahedral of FeO₆. The length increases due to the single phonon mode 541 cm⁻¹ showing the stretch mode representing the blow of the oxygen ion next to the Fe atom. The remaining call wires in 171, 269, 292, 333, 386, and 429 cm⁻¹ interlocking angles between the metal and oxygen (Fe-O) ions are a clear indication of John's Taller distortion (M. Zaghrioui, Ta Phuoc, Souza, & Gervais, 2008).

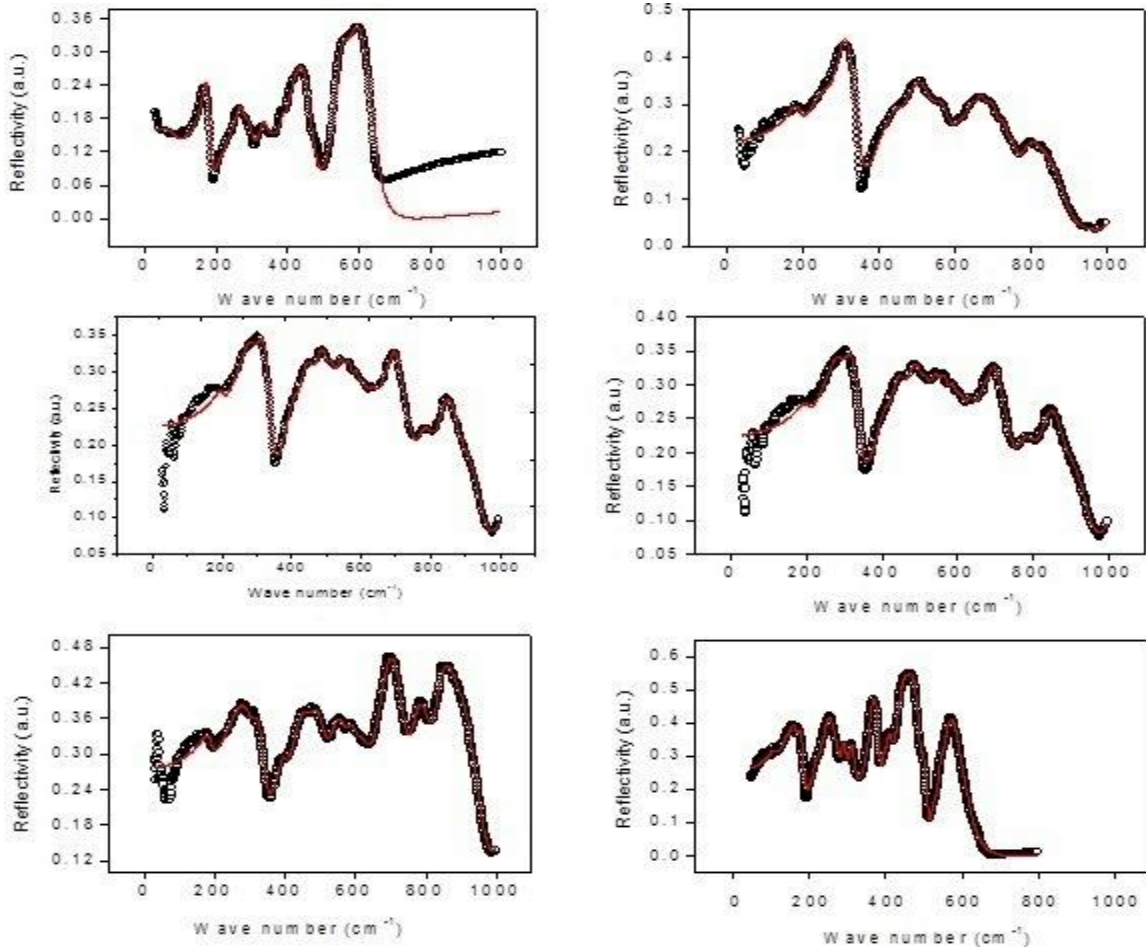


Fig. 2. Fitted reflectivity spectra of La_{1-x}Er_xFeO₃ for (x=0, 0.2, 0.4, 0.6, 0.8 and 1) at room temperature at normal incidence.

The Reflectivity spectrum of $x = 0.2$ has 11 modes, the high-resolution phonons of 580 cm^{-1} are due to the oxygen atomic movement compared to other atoms in the sample. Here the rising height indicates the stretching mode representing the binding of oxygen ions next to the Fe in the B-site atom. This category has the firmness of the first mode, the second mode softens, the next six modes harden, the continuous mode seven and eight show softness, the next nine and eleven modes also show the firmness. For $x = 0.4$, spectrum has 11 modes. At high frequency mode 580 cm^{-1} length rising appear due to single phonon exhibited the stretching mode. The spectra have actions to strengthen.

The first and third, fourth, fifth, sixth, ninth and tenth modes and the second, eighth and eleven modes have a soft character. As for $x=0.6, 0.8, 1.0$ there are 11, 12 and 14 modes respectively showing higher frequency mode at $558, 554$ and 596 cm^{-1} . The most reliable phonon optical longitudinal mode is usually predicted by the Lyddane-Sachs-Teller (LST) relation as; $\omega_{LO}^2 = (\epsilon_0/\epsilon_\infty) \omega_{TO}^2$ (Chang, 1976). Representation of the phonon longitudinal optical mode (ω_{LO}) of the phonon in table 4 and the concentration changes in the longitudinal optical modes were recorded. Phonon optical transverse mode (optical TO) as an Erbium concentration function and is calculated from the high-resolution of $\text{La}_{1-x}\text{Er}_x\text{FeO}_3$. The best suitable results related to the various parameters are listed in Table 2. The change in phonon mode to high frequencies is due to the integration of the phonons

between the levels of freedom such as the phonon-electron connection. For further examination of phonon contribution to IR spectrum of LFO, optical conductivity have calculated as $\sigma(\omega) = \omega\epsilon_2/4\pi$ by using Kramer Kronig transformation (Massa, Falcón, Salva, & Carbonio, 1997). If $\omega = 0$, then $\sigma(0) = 0$, this exhibits no free carriers participated at low energy range and hence indicates charge carriers are also localized.

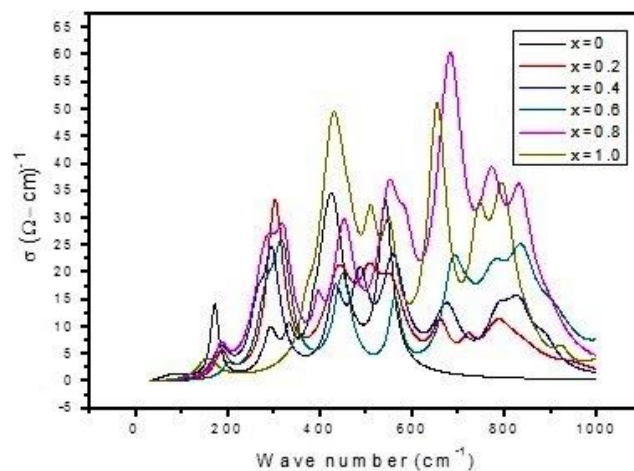


Fig. 3. Optical conductivity pattern for $\text{La}_{1-x}\text{Er}_x\text{FeO}_3$ at $(x = 0, 0.2, 0.4, 0.6, 0.8, 1.0)$.

Table 1. The value of phonon frequencies (transverse phonon frequency) obtained from fitted reflectivity spectrum for $\text{La}_{1-x}\text{Er}_x\text{FeO}_3$ by Lorentz oscillator model.

X	X = 0	X = 0.2	X = 0.4	X = 0.6	X = 0.8	X = 1
ω_{T01}	85	109	108	115	108	111
ω_{T02}			148	157	157	159
ω_{T03}	171	166	164	174	176	175
ω_{T04}		235	231	239	213	219
ω_{T05}	269	269	258		241	247
$\omega_{T05'}$						265
ω_{T06}	292	292	295	296	290	288
$\omega_{T06'}$					308	309
ω_{T07}	333	346	352	359	357	361
ω_{T08}	386	375		376	401	405
ω_{T09}	417	407	408	404		
ω_{T010}	428	434	431	433	432	431
ω_{T011}		487	459	468	460	459
$\omega_{T011'}$						495
ω_{T012}	541	580	595	558	596	554
ϵ_∞	2	1.91	1.89	2.54	2.69	2.15
ϵ_0	4.74	5.57	1.90	5.93	8.71	7.63

Table 2. Value of damping in (cm⁻¹) (dielectric simulation parameter) for La_{1-x}Er_xFeO₃.

X	X =0	X =0.2	X =0.4	X =0.6	X =0.8	X =1
γ ₁	80.98	18.71	24.98	14.66	17.27	27.09
γ ₂			21.73	26.35	34.38	21.43
γ ₃	22.05	22.86	21.25	23.9	21.82	18.98
γ ₄		39.12	22.24	24.68	12.69	18.27
γ ₅	18.01	29.12	22.19		28.99	33.29
γ _{5'}						29.68
γ ₆	38.01	35.88	31.47	16.14	29.94	18.38
γ _{6'}					21.05	21.48
γ ₇	25.24	22.59	35.2	27.2	34.05	24.12
γ ₈	13.01	19.99		32.52	33.55	22.59
γ ₉	66.01	38.32	32.47	39.97		
γ ₁₀	60.01	59.48	33.28	38.31	31.29	32.52
γ ₁₁		53.24	31.85	53.33	51.59	31.06
γ _{11'}						17.64
γ ₁₂	37.01	39.55	50.98	51.38	92.21	34.09

Table 3. The value of oscillator strengths (dielectric simulation fitting parameters) for La_{1-x}Er_xFeO₃.

X	X =0	X =0.2	X =0.4	X =0.6	X =0.8	X =1
s ₁	0.86	0.44	0.7	0.13	0.45	0.51
s ₂			0.62	0.81	1.82	0.96
s ₃	0.616	1.53	0.96	0.92	0.67	0.68
s ₄		0.74	0.34	0.45	0.11	0.14
s ₅	0.004	0.28	0.3		0.71	1.4
s _{5'}						0.26
s ₆	0.21	0.32	0.43	0.14	0.57	0.22
s _{6'}					0.16	0.26
s ₇	0.08	0.08	0.19	0.21	0.86	0.51
s ₈	0.01	0.03		0.07	0.31	0.16
s ₉	0.37	0.1	0.1	0.19		
s ₁₀	0.36	0.08	0.11	0.2	0.23	0.31
s ₁₁		0.02	0.04	0.11	0.1	0.02
s _{11'}						0.01
s ₁₂	0.23	0.02	0.008	0.16	0.03	0.04

Table 4. Longitudinal optical frequencies calculated by L.S.T for La_{1-x}Er_xFeO₃.

X	X = 0	X = 0.2	X = 0.4	X = 0.6	X = 0.8	X = 1
ω _{LO1}	130	185	107	176	195	209
ω _{LO2}			147	240	282	298
ω _{LO3}	264	283	164	265	317	329
ω _{LO4}		401	231	364	383	413
ω _{LO5}	414	458	259		433	465
ω _{LO5'}						500
ω _{LO6}	449	499	295	452	521	542
ω _{LO6'}					554	581
ω _{LO7}	512	590	352	548	641	678
ω _{LO8}	594	640		574	722	762
ω _{LO9}	641	695	409	616		
ω _{LO10}	660	740	431	661	777	812
ω _{LO11}		831	459	713	828	863
ω _{LO11'}						932
ω _{LO12}	833	991	595	852	1072	1042

Electrical properties: For analyzing the conduction mechanism, DC electrical resistivity measurement with varying temperature (300 – 393 K) for sample $\text{La}_{1-x}\text{Er}_x\text{FeO}_3$ ($x = 0.0, 0.2, 0.4, 0.6, 0.8, 1.0$) is shown in figure 4. Decrement of resistivity observed for all samples as temperature increases. These happen due to thermally activation and drift mobility of charge carriers from valence to conduction band, enhance conduction according to hopping conduction mechanism. The value of temperature depended resistivity excel with increase in Er^{+3} substitutions. It occurs due to different electronic configuration of La ($[\text{Xe}] 6s^2 5d^1$) and Er ($[\text{Xe}] 6s^2 4f^{12}$). In lanthanum d (valence orbit), having 9 vacant positions of electrons but in Er having f sub shell (valence orbit) having only 2 vacant positions. So by increasing Er concentration, there will be less vacant position, hence mobility decreases. Experimentally Er^{+3} substitution decreases conductivity. Thus chasing the Arrhenius rule having +ve slope as shown in figure 5 deducted from the relation

$$\rho = \rho_0 \exp (\Delta E / K_B T) \quad (3)$$

where ΔE is activation energy, K_B is Boltzmann constant its value is 1.38×10^{-23} J/K. Slope of $\ln \rho$ Vs $1/K_B T$ gives the activation energy for all samples. There is a decrement of activation energy of prepared from 0.73 eV to 0.17 eV, as Er^{+3} concentration increases is shown in figure 6. The calculated value of E_a is greater than 0.2 eV, is the confirmation of polaron conduction of holes (Idrees, Nadeem, & Hassan, 2010)

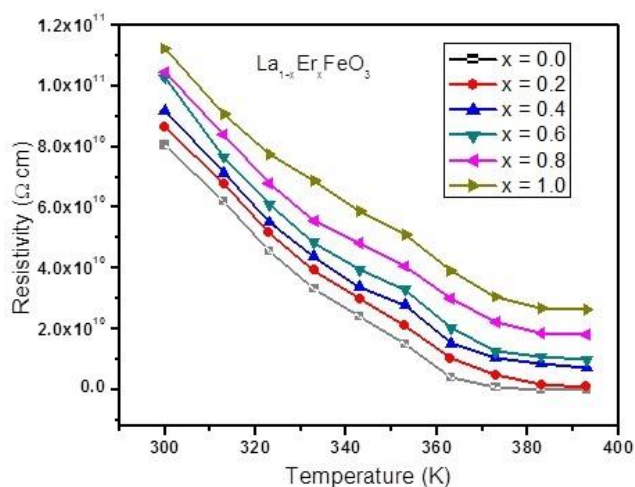


Fig. 4. Resistivity vs temperature for $\text{La}_{1-x}\text{Er}_x\text{FeO}_3$ ($X = 0, 0.2, 0.4, 0.6, 0.8, 1.0$).

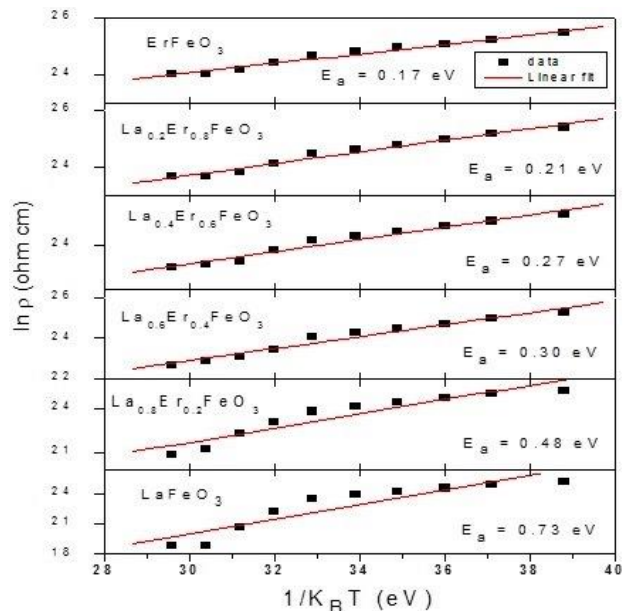


Fig. 5. Arrhenius plot for $\text{La}_{1-x}\text{Er}_x\text{FeO}_3$ at ($X = 0, 0.2, 0.4, 0.6, 0.8$ and 1).

UV-Visible Analysis: To figure out photo catalytic and optoelectronic properties, optical band gap is important tool. The realignment of different charge carriers occurs between different energy levels gives an absorption edge when optical absorption studied. The absorbance coefficient obtained from reflectance data by using Kubelka–Munk (K-M) transform (Thakur, Pandey, & Singh, 2014). The K-M function is given as:

$$F(R) = \frac{(1-R)^2}{2R} \quad (4)$$

Here $F(R)$ is used for absorbance and R is reflectance of sample. For LaFeO_3 absorbance is steadily increasing with increasing wavelength in visible spectrum. The graphical representation of $h\nu$ and $(\alpha h\nu)^{1/r}$ describe Tauc relation from equation; $\alpha h\nu = A(h\nu - E_g)^{1/r}$ and used to find optical band gap (Tauc, Grigorovici, & Vancu, 1966). Here r gives type of transition, which is $1/2$ for direct forbidden and 2 for indirect transition (Javed Ahmad *et al.*, 2017), a is absorbance co-efficient denoted by $F(R)$ also. For undoped sample LaFeO_3 value of optical band gap energy is 1.83eV, showing semiconducting behaviour. Now take sample ErFeO_3 when $x = 1.0$, Tauc plot gives value of optical band energy which is 1.97eV as shown in Figure 7 and 8. There is very minute distance between two peak position samples; hence there is no need to plot the other sample. From the literature, we know that electron exchanges occur between the 3d orbital (conduction band) of metal (Fe) and the 2p orbital (valence Band) of oxygen, so this indicates the independence of the doped object. The obtained band gap value for both samples indicates semiconducting nature of the series.

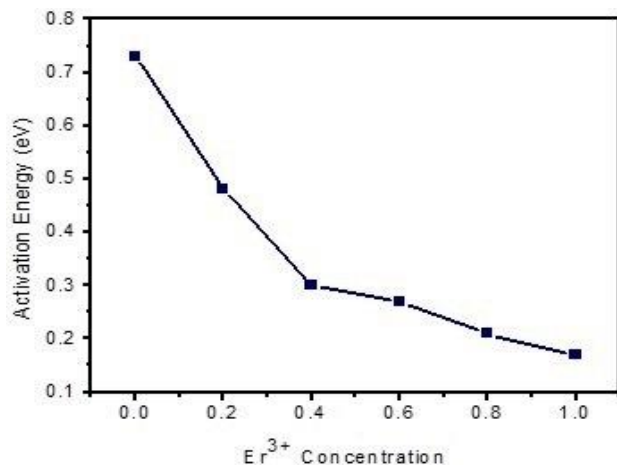


Fig. 6. Variation of activation energy with varying concentration of erbium.

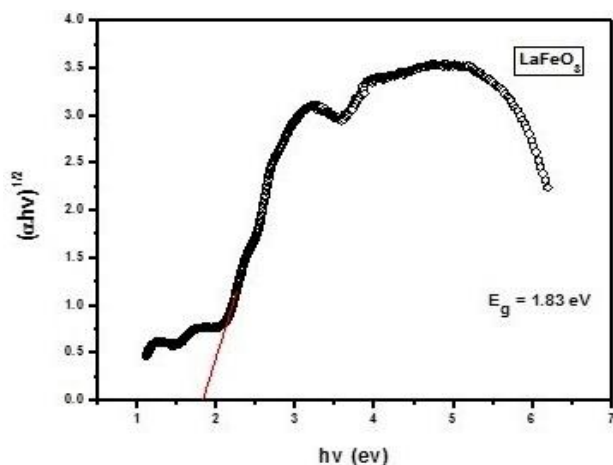


Fig. 7. Tauc Plot for LaFeO₃.

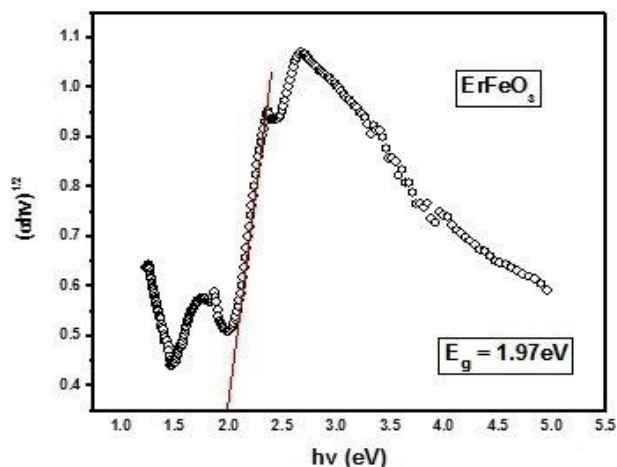


Fig. 8. Tauc Plot for ErFeO₃.

Conclusion: The optical and electrical properties of multiferroic materials La_{1-x}Er_xFeO₃ with Er³⁺ doping concentration at (x=0, 0.2, 0.4, 0.6, 0.8 and 1) have been synthesized by using sol gel method (auto combustion).

XRD results were compared with JCPDS cards that revealed the orthorhombic structure present in the samples. Quantitatively spectra are explored using Lorentz oscillator model, one of the interesting consequences is the twelve active phonons were detected which is helpful for using them as the dielectric purpose. The observed active phonons are increased with doping concentration. Splitting of phonon peaks and sharp decreasing in Lorentz oscillating strength are observed with increasing doping concentration. As the result we observed the maximum no of phonons appeared at maximum concentration that's shows the change in Fe-O ions knows as John Tellers distribution. The hardening and softening behaviour has been observed in TO and LO modes, respectively. The optical band gap measured for two samples LaFeO₃ and ErFeO₃ (having peak positions x = 0 and 1), which is 1.83 eV and 1.97 eV, respectively. The dc electrical resistivity of sample decreases with increasing temperature indicating semiconducting nature of all the samples. The activation energy of sample drops from 0.73 eV to 0.17 eV as concentration of doped element erbium increases. Here activation energy is greater than 0.2 eV recommend the p-type polaronic conduction mechanism in the system.

Acknowledgement: The financial support of the HEC, Pakistan through its NRP/No. 9301/Punjab/NRP/UR & D/HEC/ 2017 is greatly acknowledged.

REFERENCES

- Ahmad, J., Bukhari, S. H., Jamil, M. T., Rehmani, M. K., Ahmad, H., & Sultan, T. (2017). Lattice Dynamics and Transport Properties of Multiferroic DyMn₂O₅. *Advances in Condensed Matter Physics*, 2017.
- Ahmad, J., Zakia, G., Abbas, H., Bukhari, S., Nissar, U., Jamil, M., .Sultan, T. (2019). Lattice and structural distortions in gd³ substituted lamno₃: Infrared reflectivity measurements. *Journal of Ovonic Research Vol*, 15(5), 345-355.
- Alter, H., & Nakatsuji, Y. (1996). Alter HJ (1996a) The cloning and clinical implications of HGV and GBV-C. *N Engl J Med* 334: 1536-1537 Alter HJ, Nakatsuij Y, Shih JW-K, Melpolder J, Kiyosawa K, Wages J, Kim J (1996b) Transfusion-associated Hepatitis G virus infection. IX. Triennial International Symposium on Viral Hepatitis and Liver Disease, Rom 21. *J Med*, 334, 1536-1537.
- Andoulsi, R., Horchani-Naifer, K., & Ferid, M. (2013). Electrical conductivity of La_{1-x}CaxFeO_{3-δ} solid solutions. *Ceramics International*, 39(6), 6527-6531.
- Bukhari, S., & Ahmad, J. (2016). Infrared active phonons and optical band gap in multiferroic GdMnO₃

- studied by infrared and UV-visible spectroscopy. *Acta Phys. Pol. A*, 129(1), 43.
- Chang, I. (1976). Dielectric function and the Lyddane-Sachs-Teller relation for crystals with Debye polarization. *Physical Review B*, 14(10), 4318.
- Eerenstein, W., Mathur, N. D., & Scott, J. F. (2006). Multiferroic and magnetoelectric materials. *Nature*, 442(7104), 759-765. doi: 10.1038/nature05023
- Hench, L. L., & West, J. K. (1990). The sol-gel process. *Chemical reviews*, 90(1), 33-72.
- Hosseini, S. A., Sadeghi, M. T., Alemi, A., Niaei, A., Salari, D., & Leila, K.-A. (2010). Synthesis, characterization, and performance of LaZn_xFe_{1-x}O₃ perovskite nanocatalysts for toluene combustion. *Chinese Journal of Catalysis*, 31(7), 747-750.
- Huang, Q., Santoro, A., Lynn, J. W., Erwin, R. W., Borchers, J. A., Peng, J. L., . . . Greene, R. L. (1998). Structure and magnetic order in La_{1-x}Ca_xMnO₃ (0 < x < 0.33). *Physical Review B*, 58(5), 2684-2691. doi: 10.1103/PhysRevB.58.2684
- Huang, Z. J., Cao, Y., Sun, Y. Y., Xue, Y. Y., & Chu, C. W. (1997). Coupling between the ferroelectric and antiferromagnetic orders in YMnO₃. *Physical Review B*, 56(5), 2623-2626. doi: 10.1103/PhysRevB.56.2623
- Idrees, M., Nadeem, M., & Hassan, M. (2010). Investigation of conduction and relaxation phenomena in LaFeO₃. 9NiO. 103 by impedance spectroscopy. *Journal of Physics D: Applied Physics*, 43(15), 155401.
- Iliev, M., Abrashev, M., Popov, V., & Hadjiev, V. (2003). Role of Jahn-Teller disorder in Raman scattering of mixed-valence manganites. *Physical Review B*, 67(21), 212301.
- Jamil, M. T., Ahmad, J., Bukhari, S. H., & Ahmad, H. (2018). Optical phonons and its effect on physical properties of rare-earth orthoferrites RFeO₃ (R= La, Nd, Gd, Dy, Er): IR reflectivity measurements. *International Journal of Modern Physics B*, 32(21), 1850229.
- Katsufuji, T., Mori, S., Masaki, M., Moritomo, Y., Yamamoto, N., & Takagi, H. (2001). Dielectric and magnetic anomalies and spin frustration in hexagonal RMnO₃. *Physical Review B*, 64(10), 104419. doi: 10.1103/PhysRevB.64.104419
- Khan, J. A., & Ahmad, J. (2019). Double perovskite La₂CrMnO₆: synthesis, optical and transport properties. *Materials Research Express*, 6(11), 115906-115918. doi: 10.1088/2053-1591/ab4728
- Mahmood, A., Warsi, M. F., Ashiq, M. N., & Ishaq, M. (2013). Substitution of La and Fe with Dy and Mn in multiferroic La_{1-x}Dy_xFe_{1-y}Mn_yO₃ nanocrystallites. *Journal of Magnetism and Magnetic Materials*, 327, 64-70.
- Massa, N. E., Falcón, H., Salva, H., & Carbonio, R. E. (1997). Infrared reflectivity of the solid solutions LaNi_{1-x}Fe_xO₃ (0.00 < x < 1.00). *Physical Review B*, 56(16), 10178.
- Sahoo, R., Das, S., & Nath, T. (2018). Effect of rare earth site substitution on magnetic and transport properties of Ln₂CoMnO₆ (Ln= La, Sm and Gd) double perovskites. *Journal of Magnetism and Magnetic Materials*, 460, 409-417.
- Tamer, M. A., Abraime, B., Abbassi, A., Maalam, K. E., Kenz, A. E., Benyoussef, A., . . . Mounkachi, O. (2016). First-principles study of electronic, electrical and optical properties of HoMn₂O₅. *Journal of Physics: Conference Series*, 758, 012009. doi: 10.1088/1742-6596/758/1/012009
- Tauc, J., Grigorovici, R., & Vancu, A. (1966). Optical properties and electronic structure of amorphous germanium. *physica status solidi (b)*, 15(2), 627-637.
- Thakur, S., Pandey, O., & Singh, K. (2014). Structural and optical properties of Bi_{1-x}A_xFeO₃ (A= Sr, Ca; 0.40 ≤ x ≤ 0.55). *Journal of Molecular Structure*, 1074, 186-192.
- Tijare, S. N., Joshi, M. V., Padole, P. S., Mangrulkar, P. A., Rayalu, S. S., & Labhsetwar, N. K. (2012). Photocatalytic hydrogen generation through water splitting on nano-crystalline LaFeO₃ perovskite. *International journal of hydrogen energy*, 37(13), 10451-10456.
- Wang, Z. L., & Kang, Z. C. (2002). FUNCTIONAL AND SMART MATERIALS-Structural evolution and structure analysis: Academic press: Peking, China.
- Zaghrioui, M., Phuoc, V. T., Souza, R., & Gervais, M. (2008). Polarized reflectivity and lattice dynamics calculation of multiferroic YMnO₃. *Physical Review B*, 78(18), 184305.
- Zaghrioui, M., Ta Phuoc, V., Souza, R. A., & Gervais, M. (2008). Polarized reflectivity and lattice dynamics calculation of multiferroic YMnO₃. *Physical Review B*, 78(18), 184305. doi: 10.1103/PhysRevB.78.184305
- Zhang, L., Hu, J., Song, P., Qin, H., & Jiang, M. (2006). Electrical properties and ethanol-sensing characteristics of perovskite La_{1-x}Pb_xFeO₃. *Sensors and Actuators B: Chemical*, 114(2), 836-840.
- Zhang, L., Qin, H., Song, P., Hu, J., & Jiang, M. (2006). Electric properties and acetone-sensing characteristics of La_{1-x}Pb_xFeO₃ perovskite system. *Materials Chemistry and Physics*, 98(2-3), 358-362.